New Trends in Radio Astronomy in the ALMA Era:
The 30th Anniversary of Nobeyama Radio Observatory
ASP Conference Series, Vol. 476
Ryohei Kawabe, Nario Kuno, and Satoshi Yamamoto eds.

ALMA Observations of Arp 220 and Dust Continuum Measurements of High-z Galaxies

Nick Scoville,[1] Kartik Sheth,[2] Hervel Aussel,[3] Swarnima Manohar,[1] and two Cycle0 teams

[1]*Astronomy Dept. California Institute of Technology, Pasadena, CA 91125*

[2]*National Radio Astronomy Observatory, 520 Edgemont Road, Charlottesville, VA 22903, USA*

[3]*AIM Unité Mixte de Recherche CEA CNRS, Université Paris VII UMR n158, Paris, France*

Abstract. We describe preliminary results for two ALMA projects – 1) imaging the HCN(4-3) line and H26α lines in Arp 220 and 2) measurements of the dust continuum in a sample of 120 high redshift galaxies to probe the evolution of the ISM masses. The HCN observations in Arp 220 at 1/2″ resolution provide the first high resolution imaging of the dense star forming gas in this prototypical ULIRG. The HCN is seen in two clearly delineated, counter-rotating disks. The H26α emission is the first definitive probe of the star formation rate in Arp 220, avoiding obscuration by dust and contamination by AGN luminosity contributions. In the second project, the remarkable continuum sensitivity of ALMA in Band 7 is used to measure the long wavelength Rayleigh-Jeans tail of the dust emission from a sample of 120 galaxies in COSMOS at z = 0.3 to 2.2, providing estimates for the dust masses and hence, for an assumed dust-to-gas ratio, their ISM masses. This technique will enable measurements for hundreds of galaxies at high-z with observations of typically ∼10 min per galaxy. This is in contrast to CO line imaging which typically requires a few hours per galaxy even with the sensitivity of ALMA. The derived ISM masses are also subject to uncertainties in the CO-to-H2 conversion factor.

1. Introduction

ALMA provides spectacular increases in sensitivity, versatility and image fidelity over existing mm/submm facilities. Here we briefly describe two projects conducted in Cycle0 which highlight future science which will be possible when ALMA reaches its full implementation in two years.

2. High Resolution Imaging in Band 7 (345 GHz) of Arp 220

Our Cycle0 project included Band 7 imaging of both Arp 220 and NGC 6240. Here we summarize the results for Arp 220. The NGC 6240 observations, combined with CARMA 3 mm imaging will be presented by Manohar *et al.* 2013.

The ALMA band 7 observations included HCN(4-3), CS(7-6) and H26α. Fig. 1 shows the 349 GHz continuum (mostly dust emission) imaged at 0.5″resolution, clearly

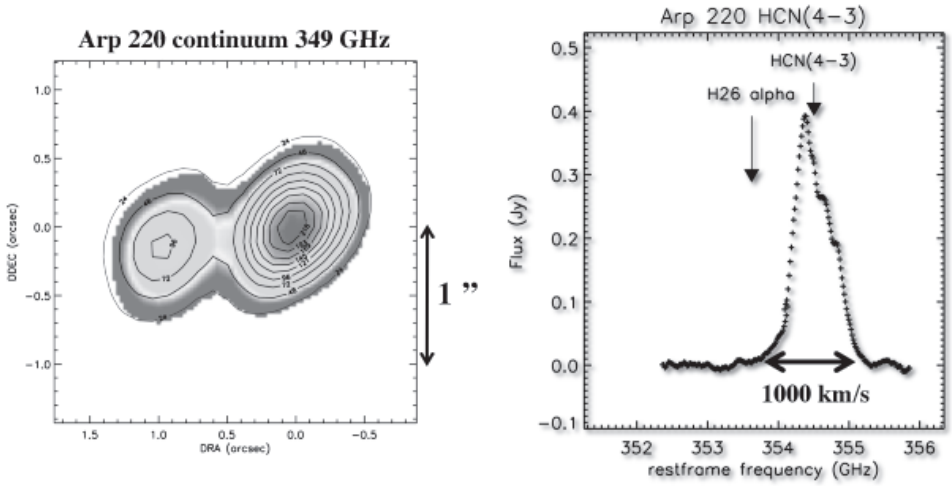

Figure 1. Left – The 349 GHz continuum image of Arp 220 at 0.5″resolution. Right – Band 7 integrated spectrum covering 352 to 356 GHz including both nuclei of Arp 220 with the continuum subtracted out. Strong HCN(4-3) emission is seen and the much weaker feature on the low frequency line wing is identified as H26α.

showing the two nuclei separated by 1″, corresponding to 300 pc. The peak brightness temperature in the continuum is approximately 10K. Allowing for partial covering in the source, this high brightness temperature suggests $\tau_{dust} \sim 1$, even at this long wavelength since the dust temperatures are likely in the range 50 - 200K (based on earlier work).

The HCN(4-3) integrated emission and mean velocity are shown in Figure 2. The western nucleus shows approximately twice as much HCN emission as the east, similar to the relative fluxes seen in CO. This HCN line has a critical density $\sim 10^6$ cm^{-3} for collisional excitation. The velocities clearly show the counter-rotating nuclear disks in each nucleus as first detected by Sakamoto et al. (1999).

Lastly, we show in Figure 3 the integrated spectra for H26α on each of the nuclei. The line is detected on the west nucleus. The low n HI recombination lines provide a proportional measure of the total ionized gas emission measure ($EM = n_e^2 volume$) and hence the Lyman continuum emission rate of young OB stars. Detecting this line was a major goal of our ALMA observations since it provides a measure of the star formation rates at a wavelength where dust obscuration is likely to be minimal. The observed flux implies a SFR $\sim 150\ M_\odot$ yr^{-1} in the western nucleus.

3. Long Wavelength Dust Continuum as an ISM Mass Tracer

The FIR-submm emission from galaxies is dominated by dust re-radiation of the luminosity from young stars and active galactic nuclei (AGN), absorbed at shorter wavelengths. The luminosity at the peak of the FIR is thus often used to estimate the luminosity of obscured star formation. Equally important (but not often stressed) is the fact

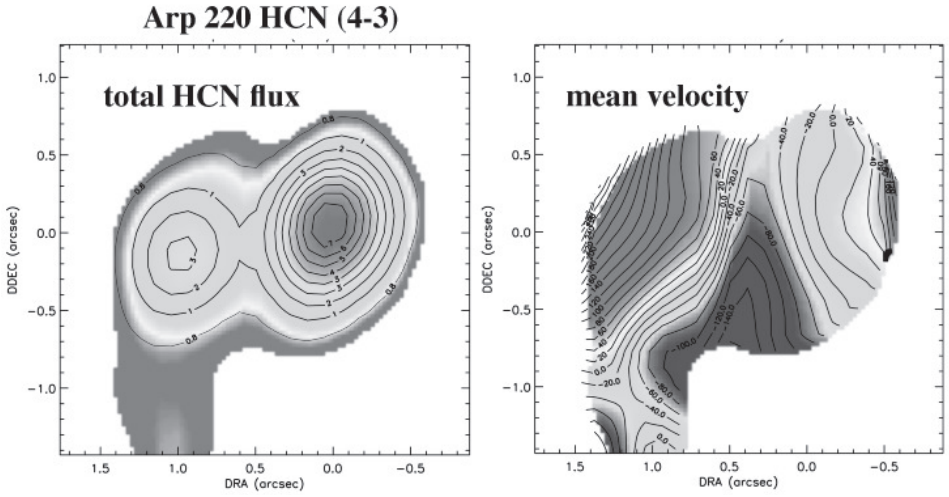

Figure 2. The total velocity-integrated HCN(4-3) emission and the velocity centroid are shown for Arp 220.

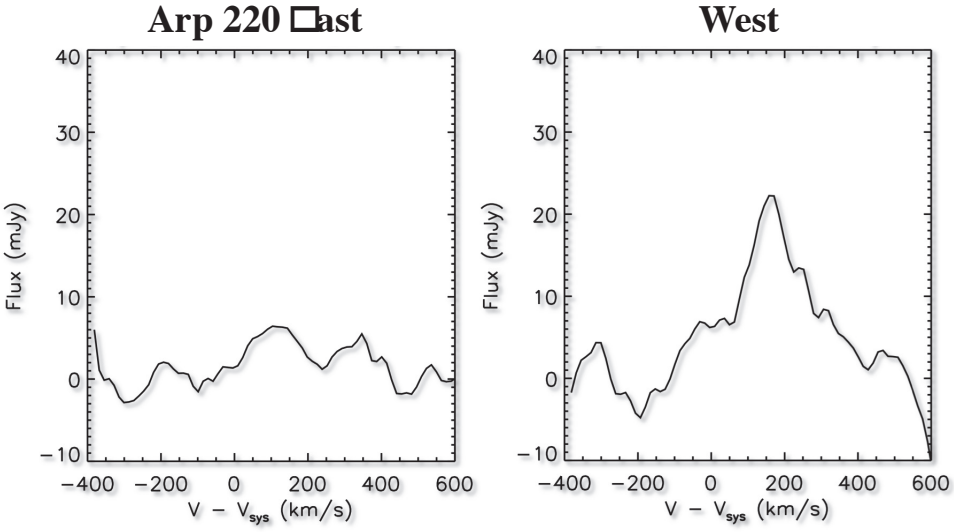

Figure 3. The spectra of H26α integrated over the areas of the East and West nuclei. The line is detected on the West nucleus.

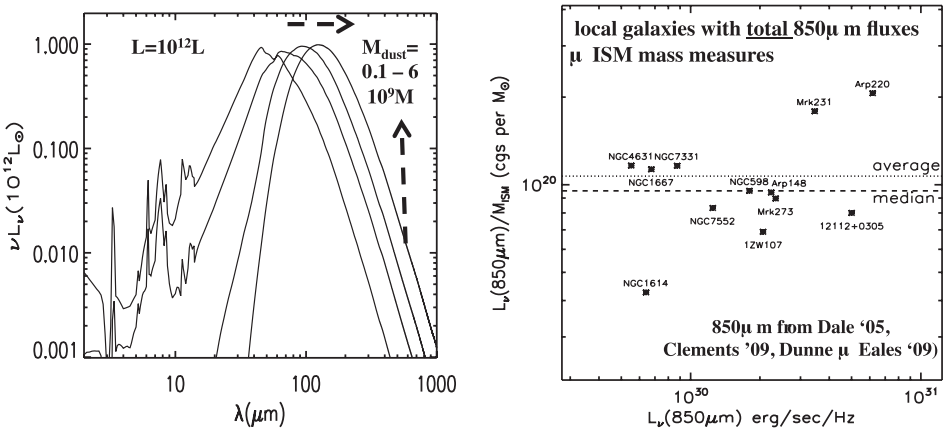

Figure 4. Left panel – Dust radiative transfer model SEDs are shown for optically thick sources with fixed luminosity but varying M_{dust}. The radiative transfer is basically a single parameter problem with the ratio L/M being the determinant for the output SED (Scoville 2012). As the dust mass is increased (or L/M is decreased), the dashed arrows show that the peak shifts to longer wavelength (due to absorption at wavelengths shorter than the peak) and the flux on the 'Rayleigh-Jeans' tail increases linearly with M_{dust}. Right Panel – The ratio of L_ν at 850μm to M_{ISM} is shown for a sample of low z spiral and starburst galaxies from Dale et al. (2005) and Clements et al. (2010). The average and median values for the sample are shown by horizontal lines.

that the long-wavelength, Rayleigh-Jeans (RJ) tail of dust emission is nearly always optically thin and thus **provides a direct probe of the dust (and hence ISM) masses**. To translate the long wavelength fluxes into an ISM mass estimate requires knowledge of the dust opacity per unit mass or equivalently an empirically derived flux to mass ratio based on local galaxies. Fortunately, the latter is well established from observations of nearby galaxies (e.g. Draine et al. 2007; Galametz et al. 2011) (and partially from theory (Draine & Li 2007)).

The standard paradigm for the far infrared emission from galaxies is a luminous source of short wavelength luminosity (a single star, a star cluster or a starburst region) which is centrally located inside an optically thick dust cloud. The innermost dust absorbs the short wavelength radiation, reradiates it at longer wavelength, and this secondary radiation heats the dust further out. A detailed model for this is described in Scoville (2012). There, it is pointed out that the dust temperature falloff with radius can be modeled in two limits: optically thin with $T \propto r^{-2/5}$ and optically thick with $T \propto r^{-1/2}$. Having these two analytic approximations, it is then easy to calculate the emergent spectral energy distribution of the far infrared radiation as seen from the outside. The emergent SEDs are basically dependent on a single parameter, the luminosity-to-mass ratio – $L_{central}/M_{dust}$ if the dust opacity properties are fixed. Sample SEDs are shown in Fig. 4-Left. There the luminosity was held fixed while the dust mass was varied over a factor 60. As the mass is increased, the wavelength at the peak shifts to longer wavelength (due to absorption on the short wavelength side of the peak) and the flux on the long-wavelength tail varies linearly with increasing mass.

On the optically thin, Rayleigh-Jeans tail of the IR emission, the observed flux density is given by :

$$F_\nu = \kappa_\nu T_{\rm dust} \nu^2 M_{\rm dust}(1+z)/(4\pi d_l^2) \quad (1)$$

where $T_{\rm dust}$ is the temperature of the emitting dust grains, κ_ν is the dust opacity per unit mass, $M_{\rm dust}$ is the total mass of dust and d_L is the source distance. In nearby, normal star-forming galaxies, the majority of the dust is at $\sim$ 20 $\rightarrow$ 25K, and even in the most vigorous starbursts like Arp 220 the FIR/submm emission is dominated by dust at temperatures $\leq$ 45K. Thus the expected variations in $T_{\rm dust}$ have less than a factor 2 effect on the observed flux.

The rest of the terms in Eq. 1 can be calibrated from submm observations of nearby galaxies. In selecting local galaxies on which to base this empirical approach, it is vital that both the submm fluxes and ISM masses are global values (or at least refer to the same areas in the galaxies). For nearby galaxies this can be a problem due to their large sizes. As a reliability check on the submm measurements we have required two long wavelength flux measurements which yield reasonable spectral indexes β (e.g. between 450 and 850μm). Our local galaxy sample includes SCUBA data for 12 galaxies – 3 from the SINGS survey (Dale et al. 2005) and 9 from ULIRGs survey (Clements et al. 2010). The ULIRG sample is in fact probably most relevant since these galaxies are closer in IR luminosity to observed high redshift galaxies and very importantly, their emission is compact so we can be confident that the total 850μm flux and ISM masses encompass the same regions. The 850μm fluxes were converted to specific luminosity at 850μm ($L_{\nu(850)}$) and ratioed to the ISM masses (HI & H_2) (see Fig. 4-Left). Based on the data shown in Fig. 4-Right, we adopt a constant of proportionality between the 850μm specific luminosity and the ISM mass,

$$\alpha_{850} = \frac{L_{\nu_{850}}}{M_{ISM}} = 1 \times 10^{20} ergs/sec/Hz/M_\odot \, . \quad (2)$$

In order to predict the observed Band 7 fluxes for high redshift galaxies, it is also necessary to adopt a spectral index β (S_ν varying as ν^β) for the restframe RJ emission. Observed 450μm/850μm flux ratios in submm galaxies indicate β between 3 and 4. For most dust models the spectral index of the opacity is typically 1.5 to 2, implying β = 3.5 to 4 (adding in the index +2 for the RJ tail). Empirical fits to the observed long wavelength SEDs give 3.5 to 4 for local galaxies (Dunne & Eales 2001; Clements et al. 2010) . For high z submm galaxies, the spectral index can be between 3.2 and 3.8 but in some cases the shorter wavelength point is getting close to the IR peak in the rest frame and therefore not strictly on the RJ tail.

Normalizing to $M_{ISM} = 2 \times 10^{10} M_\odot$ and adopting $\beta = 3.8$,

$$S_{\nu_{obs}} = \alpha_{850} \, \frac{M_{ISM}}{2 \times 10^{10} M_\odot} \, (1+z)^{4.8} \, \frac{\nu_{obs}}{350}^{3.8} \, \frac{1}{4\pi d_L^2} \quad (3)$$

$$S_{\nu_{obs}}(mJy) = 1.67 \, \frac{M_{ISM}}{2 \times 10^{10} M_\odot} \, (1+z)^{4.8} \, \frac{\nu_{obs}}{350}^{3.8} \, \frac{1}{d_L^2(Gpc)} \quad (4)$$

The curves in Figure 4-Left show the predicted continuum fluxes as a function of redshift for both Band 7 (347GHz) and Band 6 (240 GHz). The expected fluxes on Fig. 4 for z = 2 are $\sim$1.7 and 0.3 mJy respectively for 2×10^{10} $M_\odot$. ALMA, with 7.5 GHz

BW in each polarization and 10 min of integration in Cycle 1 yields σ = 0.068 mJy at 345 GHz and σ = 0.045 mJy at 240 Ghz. It is thus clear that Band 7 is favored since the expected flux ratio is ∼5:1 whereas the sensitivity ratio is less than 2:1.

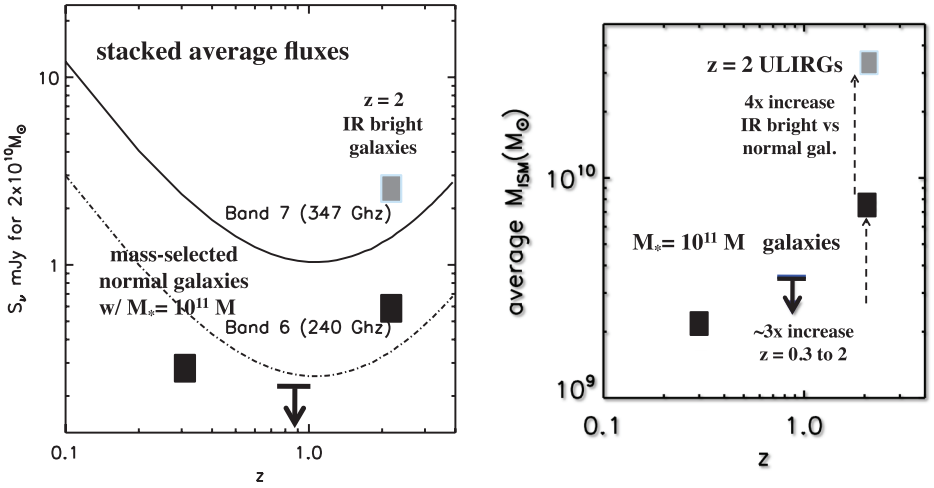

Figure 5. For of the four samples of galaxies (stellar mass selected at $10^{11} M_\odot$ and z = 0.3, 0.3 and 2, and IR-bright at z =2) we show the average fluxes for each sample (Left panel) and inferred ISM masses (Right panel). The curves on the left panel show the variation in the expected flux for ALMA Bands 6 and 7 for a constant ISM mass of $2 \times 10^{10} M_\odot$. For the z = 0.8 sample, only an upper limit is obtained but this redshift is at the minimum predicted fluxes due to the increasing luminosity distance and the fact that the negative k-correction doesn't help much until after z ∼ 1.

In our Cycle0 project we had 5 hrs of integration time in Band 7 to observe four samples of galaxies. There were three samples at z = 0.3, 0.9 and 2 consisting of 38, 33 and 38 galaxies, respectively. They were all in the COSMOS survey field and mass-selected to have stellar masses of $10^{11} M_\odot$. They were not selected to be IR luminous. An additional 6 galaxies which are IR luminous (ULIRGs) at z = 2.2 were also observed for comparison to see if they had more ISM or simply a higher efficiency for forming star but the same mass of ISM. The stacked average fluxes of the four samples are shown in Fig. 5-Left. Their inferred ISM masses are shown in Fig. 5-right. This very preliminary investigation shows quite clear increase by a factor 3 in the dust and iSM masses going from z = 0.3 to 2 in the mass-selected galaxies. At the same time, the IR luminous galaxies at z = 2 have ∼ 4 times larger ISM masses than the sample at the same redshift but purely mass-selected. In Fig. 6, the Band 7 continuum images are shown for two of the brighter z = 2 galaxies together with 2.2μm continuum images.

Lastly, we address the issue of variation in the dust-to-gas ratio and its dependence on metallicity. Seventeen of the nearby SINGS survey galaxies have good total submm flux measurements (see Draine et al. 2007), as well as good measurements of the total molecular (H_2) and atomic (HI) gas masses. Over a range of ∼0.5 dex down in metallicity from the Milky Way, there is little evidence of variation in the dust-to-gas mass ratios, while at still lower metallicity the dust abundance does decrease. Therefore, as long as one stays with samples of high metallicity galaxies (i.e. high stellar mass galaxies), the scaling between RJ tail flux and ISM mass should remain valid. [At the lower metallicities, the SINGS galaxies do not have total SCUBA 850 μm fluxes and

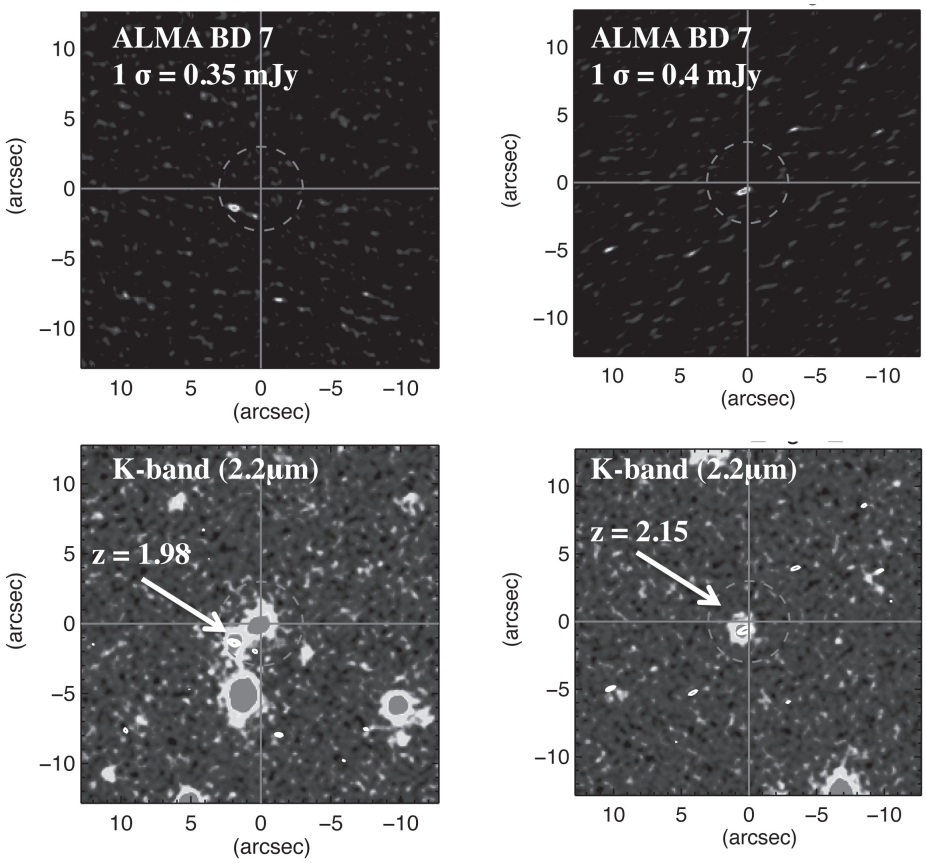

Figure 6. Postage stamps of the ALMA Band 7 continuum detections and 2.2μm images for two z = 2 galaxies detected in our Cycle0 COSMOS dust continuum project. The measured fluxes are 1.6 - 4.3 mJy.

the submm fluxes must be estimated from an overall SED fit using shorter wavelength observations; for these lower metallicity galaxies, there is evidence for a decrease in the dust-to-gas ratio (see Draine et al. 2007).]

These initial Cycle0 results using the long wavelength flux measures to probe iSM evolution and variations in the ISMs of different galaxy samples at high-z, show great promise. The completed ALMA will be more than a factor 3 increased in sensitivity, enabling such detections within a few minutes in samples of ordinary galaxies.

Detecting the fiducial ISM mass of $2 \times 10^{10} M_{\odot}$ (1.7 mJy in Band 7) at 5σ requires only a few minutes of integration at Cycle 1 sensitivity. One can compare this with the time required to measure the same mass using the CO line, e.g. redshifted CO (3-2) in the Band 3. Using line fluxes from Tacconi et al. (2010), the average line flux averaged over a single resolution element of 300 km/s would be 0.28 mJy, and detecting this same mass in CO at 5σ would require $\sim$ 3 hrs at ALMA Cycle1 sensitivity.

Acknowledgments. We would like to thanks our hosts for organizing a most enjoyable and stimulating meeting in beautiful Hakone.

References

Clements, D. L., Dunne, L., & Eales, S. 2010, MNRAS, 403, 274. 0911.3593

Dale, D. A., Bendo, G. J., Engelbracht, C. W., Gordon, K. D., Regan, M. W., Armus, L., Cannon, J. M., Calzetti, D., Draine, B. T., Helou, G., Joseph, R. D., Kennicutt, R. C., Li, A., Murphy, E. J., Roussel, H., Walter, F., Hanson, H. M., Hollenbach, D. J., Jarrett, T. H., Kewley, L. J., Lamanna, C. A., Leitherer, C., Meyer, M. J., Rieke, G. H., Rieke, M. J., Sheth, K., Smith, J. D. T., & Thornley, M. D. 2005, ApJ, 633, 857. arXiv:astro-ph/0507645

Draine, B. T., Dale, D. A., Bendo, G., Gordon, K. D., Smith, J. D. T., Armus, L., Engelbracht, C. W., Helou, G., Kennicutt, R. C., Jr., Li, A., Roussel, H., Walter, F., Calzetti, D., Moustakas, J., Murphy, E. J., Rieke, G. H., Bot, C., Hollenbach, D. J., Sheth, K., & Teplitz, H. I. 2007, ApJ, 663, 866. arXiv:astro-ph/0703213

Draine, B. T., & Li, A. 2007, ApJ, 657, 810. arXiv:astro-ph/0608003

Dunne, L., & Eales, S. A. 2001, MNRAS, 327, 697. arXiv:astro-ph/0106362

Galametz, M., Madden, S. C., Galliano, F., Hony, S., Bendo, G. J., & Sauvage, M. 2011, A&A, 532, A56. 1104.0827

Sakamoto, K., Scoville, N. Z., Yun, M. S., Crosas, M., Genzel, R., & Tacconi, L. J. 1999, ApJ, 514, 68. arXiv:astro-ph/9810325

Scoville, N. Z. 2012, ArXiv e-prints. 1210.6990

Tacconi, L. J., Genzel, R., Neri, R., Cox, P., Cooper, M. C., Shapiro, K., Bolatto, A., Bouché, N., Bournaud, F., Burkert, A., Combes, F., Comerford, J., Davis, M., Schreiber, N. M. F., Garcia-Burillo, S., Gracia-Carpio, J., Lutz, D., Naab, T., Omont, A., Shapley, A., Sternberg, A., & Weiner, B. 2010, Nat, 463, 781. 1002.2149